

Experimental study on the bond behaviour of a transversely compressed mechanical anchorage system for Externally Bonded Reinforcement

Cristina Barris¹, Luis Correia², José Sena-Cruz²

¹ AMADE, Polytechnic School, University of Girona, Girona, Spain

² ISISE, Dept. of Civil Engineering, University of Minho, Azurém, Guimarães, Portugal

Abstract

This paper presents an experimental programme aiming at studying the bond behaviour of carbon-FRP (CFRP) for externally bonded reinforcement (EBR) systems mechanically anchored to concrete. Eleven large scale pull-out tests were carried out using concrete blocks of 200 mm × 500 mm × 800 mm. In each block a single CFRP laminate was mounted using the EBR technique and mechanically fixed to concrete through a commercial mechanical anchorage with different levels of transverse compression. The blocks were tested under a pull-out configuration until failure. The study of the CFRP EBR system comprises not only the mechanical anchorage but also the subsequent CFRP EBR laminate bonded to concrete. The debonding load is observed to be dependent on the laminate width, as expected, and a good relationship between the experimental results and analytical predictions is found. A model of the local bond shear stress-slip law in the bonded zone is adopted and calibrated to the experimental results taking into account the roughness of the concrete surface. Moreover, the effects of the laminate width and the compressive stress level on the anchorage effectiveness are evaluated. Results show that the mechanical anchorage generally provides adequate transverse compression of the CFRP laminate to concrete surface.

Keywords: bond behaviour, CFRP, EBR, transverse compression

1. Introduction

Fibre reinforced polymers (FRP) have emerged as technical and economically viable materials for strengthening applications of reinforced concrete (RC) elements in countless applications worldwide [1–3].

30 Different strengthening techniques have been developed with FRP, being the most commonly used (i)
31 the externally bonded reinforcement (EBR) technique, and (ii) the near-surface mounted (NSM)
32 technique. The EBR technique consists on gluing the FRP laminate on the tensile face of the RC
33 element; whereas in the NSM technique the FRP strip or bar is inserted onto a groove previously cut in
34 the concrete cover, and then is bonded to concrete with an appropriate groove filler. Epoxy adhesives
35 are typically used as bonding agents in the EBR and the NSM technique. Several premature debonding
36 failure modes have been reported in the literature for RC elements strengthened in flexure using FRP
37 laminates [4]: concrete cover separation failure and plate interfacial debonding are typically developed
38 at the laminate's extremities; whereas the intermediate crack-induced debonding (IC debonding) and
39 shear induced debonding (also referred as critical diagonal crack debonding) initiate away from the
40 laminate ends [4]. The bond behaviour between FRP and concrete is generally a critical issue as it is
41 shown by the significant number of studies found in the literature for both EBR [4–13] and NSM
42 [6,12,14–17] techniques.

43 In some structural applications, the use of prestressed FRP reinforcement is convenient or even
44 required. By prestressing the FRP material, the benefits of the EBR technique are combined with the
45 advantages associated with external prestressing, mainly [8]: more efficient use of the FRP and
46 concrete; deflection and crack width reduction, internal steel reinforcement strains relieved, higher
47 fatigue resistance and increase of the ultimate capacity resistance among other advantages. In those
48 applications with prestressed FRP reinforcements, special end anchorages are frequently used in order
49 to transfer the high shear stresses, typically developed between the FRP reinforcement and the
50 concrete, for the sake of avoiding undesirable premature FRP peeling-off failure [5,9]. Several
51 anchorage devices can be already found in the literature, and can be classified into [4,18,19]: i) U-
52 jacked anchors [20–23], ii) mechanically fastened metallic anchors [24–28], iii) FRP anchors [29–35]
53 and iv) gradient anchorage [19,36,37]. Among them, mechanical anchorages have been demonstrated
54 to be one of the most effective form of FRP anchorage device when applied to flexural strengthening,
55 e.g. [4].

56 The effectiveness of mechanical anchorages to prevent premature failure in RC flexural elements
57 strengthened with prestressed EBR CFRP laminates has been previously reported in the literature [38–
58 42]. In most of the cases, debonding of (the adhesively bonded) CFRP laminate from the concrete,
59 followed by the rupture of the laminate was attained [38]; however, a recent study with over fourteen

60 RC slabs strengthened with EBR prestressed CFRP laminates reported a premature failure by end
61 debonding at the mechanical anchorage [40,41].

62 A relationship between the level of compressive stresses provided by the anchorage device and the
63 tensile capacity of the system should be expected, as it enables friction in the cracked interface and, as
64 a result, increases the load capacity of the anchorage [43]. It is well-known that the load capacity of an
65 EBR anchorage without compressive stresses is limited by its effective bond length [44]. Nevertheless,
66 when compressive stresses are applied, the concept of effective bond length is no longer suitable. In
67 this case, the maximum anchorage capacity will be also dependent on its length. The imposed
68 compressive stresses are responsible for the development of residual bond shear stresses. Consequently
69 after the anchorage failure (by laminate slippage), the resisting load does not decrease to zero, but does
70 to a fixed residual value that varies with the anchorage length and level of compressive stress [45].

71 The present paper aims at contributing to a better understanding of the bond behaviour of CFRP EBR
72 systems mechanically anchored to concrete through an experimental study. Compressive stress
73 provided by a commercial mechanical anchorage for the bond shear stress-slip response of an EBR
74 CFRP-concrete joint is studied and the outcomes of the experimental results are presented and
75 discussed. The study of the CFRP EBR system comprises not only the mechanical anchorage but also
76 the subsequent EBR CFRP laminate, as typically found in an EBR intervention. The results from the
77 large scale pull-out tests are compared with the prediction from the literature, analysed and discussed.
78 In addition, a model of the local bond shear stress-slip law in the bonded zone is adopted and calibrated
79 to the experimental results. Finally, the effects of the level of compressive stresses through the torque
80 applied and the laminate width on the anchorage effectiveness are evaluated.

81

82 2. Experimental programme

83 The experimental programme involved eleven prismatic concrete specimens of 200 mm × 500 mm ×
84 800 mm. In these blocks, CFRP laminates were installed according to EBR technique and were
85 mechanically anchored to the concrete substrate through an aluminium plate torqued to the concrete.
86 Two main parameters were studied: (i) the laminate width (50, 80 and 100 mm), and (ii) the level of
87 compressive stresses through the torque that was applied in the anchorage plate bolts (30, 100, 150 and
88 200 N·m). Regarding to the former parameter, the selected values are in agreement with the typical
89 geometries of laminates used with this anchorage system. For the case of later parameter, the value of

90 200 N·m was defined based on limitations of usual chemical bolt-concrete systems (used to fix the
91 anchorage plate), which yielded to a compressive stress level up to approximately 30 MPa. It should be
92 highlighted that preliminary compression tests (in the transverse direction) on CFRP samples were
93 performed up to 80 MPa, based on the mechanical properties of the CFRP laminates used. These tests
94 revealed no signs of damage on the composite material. Values of torque of 150 N·m are currently used
95 in applications at structural level, e.g. [40,41]. A negligible value of torque (30 N·m) was also
96 considered in the present study, as well as an intermediate value between these last two mention
97 torques. All specimens are labelled with a generic denomination: LX_TY, where X indicates the
98 laminate width in [mm] (50, 80 or 100), and Y stands for the torque level applied in the anchorage
99 plate bolts in [N·m] (30, 100, 150 and 200).

100

101 **2.1. Materials**

102 The concrete strength was C30/37 with an exposure class of XC4(P) according to Eurocode 2 [46],
103 with a maximum aggregate size of 12.5 mm. The concrete compressive strength and modulus of
104 elasticity were assessed using compression tests following NP EN 12390-3:2011 [47] and LNEC E397
105 1993:1993 [48] recommendations, respectively. From the six cylindrical specimens tested (150
106 mm/300 mm), a mean compressive strength of 33.3 MPa with a coefficient of variation (CoV) of
107 1.31% and a mean modulus of elasticity of 24.7 GPa (CoV=5.26%) were obtained.

108 The CFRP used in this experimental work was a prefabricated pultruded laminate strip distributed by
109 from S&P Company [31]. This laminate strip (type S&P laminate CFK) was made of unidirectional
110 carbon fibres (fibre volume content is higher than 68%) assembled together by an epoxy vinylester
111 matrix. Three different widths (50, 80, and 100 mm) with a constant thickness of 1.2 mm were tested.
112 Their tensile mechanical properties were obtained from six samples tested following the procedures
113 included in ISO 527-5:2009 [49], and are summarised in **Table 1**. All specimens presented an
114 explosive failure type, by rupture of the fibres located at the middle of the test sample.

115 The two-component epoxy S&P resin 220 was used to bond the CFRP laminate strips to the concrete
116 surface. According to the manufacturer, after mixing the two components, the homogenized compound
117 density is 1.70-1.80 g/cm³ and has the following mechanical properties: compressive strength >70
118 MPa; tensile E-modulus >7.1 GPa; shear strength >26 MPa; adhesive tensile strength to concrete or
119 CFRP laminate >3 MPa (after 3 days of curing at 20 °C). In the scope of the present work the epoxy

120 adhesive was not characterized; however, a previous experimental programme reported a modulus of
121 elasticity of 7.2 GPa (CoV=3.7%) and a tensile strength of 22.0 MPa (CoV=4.5%), after 7 days of
122 curing at 22 °C [50].

123

124 **2.2. Preparation of specimens**

125 **The present** experimental programme aimed at investigating the bond behaviour of a mechanical
126 anchorage (MA) system for EBR strengthening technique. **For that purpose the specimen configuration**
127 **was conceived in order to accommodate the anchorage and EBR components. This option assures**
128 **better representativeness of the real applications and allows better understanding of the bond behaviour**
129 **in the transition between the EBR and anchorage components. Thus,** the following procedure was
130 implemented in all specimens (**Figure 1**):

131 (1) The surface roughness of the concrete was restored and enhanced with a sandblasting
132 technique. Six holes with a diameter of 18 mm and a total depth of 150 mm were drilled on
133 the concrete surface to allocate the metallic anchor bolts.

134 (2) After sandblasting and drilling, the holes and the concrete surface were carefully cleaned by
135 using pressurized air.

136 (3) The metallic anchor bolts were glued with HIT-HY 200-A® **which is a** chemical bond agent
137 to fix each aluminium anchorage plate.

138 (4) The bi-component epoxy resin was prepared according to the requirements provided by the
139 supplier. The CFRP laminate strip was properly cleaned with a solvent and the adhesive was
140 applied on the surface of the CFRP laminate, with a target minimum regular thickness of
141 1.5 mm along a total length of 272 mm (corresponding to the length of the plate) plus 250 mm
142 (which was considered an adequate upperbound value for the bonded length of the laminate
143 according to formulations suggested by technical literature, [51], in order to exceed the
144 effective bond length).

145 (5) A similar epoxy layer was applied on the cleaned concrete surface and the laminate was
146 carefully placed centred on the surface of the concrete block.

147 (6) The surface of the anchorage plate was slightly grinded with sandpaper and cleaned with a
148 solvent before applying the same batch of epoxy resin that was applied on the CFRP laminate
149 and the concrete.

150 (7) Then, the metallic plate, which had 6 holes of 18 mm diameter to accommodate 6 bolt anchors
151 of 16 mm, was placed on its predefined location.

152 (8) Just after the mechanical anchorage was placed in its correct place, it was torqued to the
153 concrete element with the aid of a dynamometric key that ensured the target level of
154 compressive stress (torque level of 30, 100, 150 and 200 N·m).

155 (9) After a curing time of 7-14 days, the specimens were ready to be tested. Aluminium tabs were
156 glued at the end of the laminate for not damaging the CFRP when hold by the clamping
157 system.

158 The anchorage plates are a commercially available solution from the same company that supplied the
159 CFRP laminate strip and epoxy resin for the end-anchorage of a CFRP laminate prestressing system. A
160 2D drawing of the anchorage plate is presented in **Figure 2**. With the dimensions of 200 mm (height)
161 by 272 mm (width) and a thickness of 12 mm, the metallic plate is made of hard aluminium and has 6
162 major holes (diameter of 18 mm) meant to accommodate M16 anchorage bolts. This aluminium plate
163 also presents 12 additional threaded holes (4 M8 and 8 M12) that are used for the prestressing system.
164 Two different types of anchor bolts were used in this experimental programme: M16 grade 8.8 for a
165 predefined torque level of 30 N·m, 100 N·m and 150 N·m, and M16 10.9 for the torque level of
166 200 N·m.

167 It is commonly accepted that the bond stress of the interface concrete-FRP highly depend on the
168 concrete roughness [10,44,52]. For that purpose, the concrete roughness characteristics after
169 sandblasting procedure were measured in all blocks at three different locations (one at the middle of the
170 bonded length, and two on the metallic anchorage zone) with a laser sensor, each sample with a total
171 length of 150 mm. The properties of the measuring device are further detailed in [40].

172 Up to now, there is not a standard parameter to evaluate the concrete roughness in EBR applications,
173 reason why in the current work the concrete roughness was evaluated following the Model Code 2010
174 [44]. Three parameters are generally used to evaluate the surface roughness on concrete-to-concrete
175 interfaces [44]: the average roughness R_a , the root mean square R_q and the peak to valley height R_t . The
176 average roughness R_a was defined as the average deviation of the surface profile from the mean line,
177 and was calculated according to,

$$R_a = \frac{1}{l} \int_0^l |y(x) - \bar{y}| dx \quad (1)$$

178 where l is the length of the measurement, $y(x)$ is the profile height at position x and \bar{y} is the mean line.
179 The root mean square R_q was defined as the square root of the arithmetic mean of the squares of each
180 profile height $(y_i - \bar{y})$ for the number of scan readings n and was computed according to Eq. (2).

$$R_q = \sqrt{\frac{1}{n} \cdot \sum_{i=1}^n (y_i - \bar{y})^2} \quad (2)$$

181 The peak to valley height R_t was defined as maximum peak-to-valley-deviation in each assessment
182 lengths. According to Model Code 2010 [44], the results obtained in **Table 2** correspond to a smooth
183 surface roughness. Only in 3% of the assessed lengths, a peak-to-valley-deviation higher than 3 mm
184 (rough surface roughness) was observed. It is worth emphasising that in concrete-to-concrete interfaces
185 the Model Code 2010 [44] categorisation (very smooth, smooth, rough and very rough) is useful for
186 design proposes (shear resistance). However, in EBR applications a different categorisation should be
187 considered, taking into consideration recent studies on this subject [10,11,40].

188

189 **2.3. Test set-up and instrumentation**

190 **Figure 3** shows the test set-up used for the large scale pull-out tests. In order to study the transition
191 from the debonding of the EBR CFRP laminate to the mechanical anchorage action, a total length of
192 522 mm of CFRP laminate was glued on the concrete surface: 272 mm corresponded to the length of
193 the metallic anchorage plate, and 250 mm were assumed to be a bonded length.

194 The concrete specimens were firstly placed onto the floor against a metallic plate with a length of 60
195 mm, which was assumed to be a rough measure of a hypothetical neutral axis depth for the case of a
196 flexural member of 200 mm height. Next, the specimens were fixed to the strong floor through a
197 metallic profile located at the top rear part of the specimen, 50 mm apart from the bottom face of the
198 block (see **Figure 3**). Once the concrete blocks had been correctly placed and fixed, the CFRP laminate
199 were connected to the hydraulic actuator through a metallic clamp specially designed for these tests.

200 The test was displacement controlled at a constant rate of 0.30 mm/min until the total debonding of the
201 laminate in the EBR bonded length (250 mm) was achieved; at that point, where the speed was
202 increased up to 2 mm/min until the end of the test.

203 The relative displacement of the CFRP laminate with respect to the concrete block was acquired by
204 means of linear variable differential transformers (LVDT) placed at different locations (**Figure 3b**): (i)
205 at the location where the CFRP laminate starts to be bonded to the concrete (loaded end, LVDT-1), (ii)

206 at the side of the anchorage plate that the laminate is pulled (mid end, LVDT-2) and (iii) at the other
207 side of the anchorage plate (free end, LVDT-3). The LVDT-1 has a range of ± 5.0 mm and a linearity
208 error of $\pm 0.24\%$, whereas the LVDT-2 and LVDT-3 range of ± 2.5 mm and a linearity error of $\pm 0.24\%$.
209 The load cell used has a maximum measuring capacity of 300 kN and a linear error of $\pm 0.05\%$. The
210 evolution of the strain profile in the laminate was registered by strain gauges (S1 to S5, TML PFL-30-
211 11-3L) placed every 62.5 mm that were glued along the CFRP bonded length.

212

213 3. Experimental results analysis and analytical predictions

214 As previously described, in the large scale pull-out tests one extremity of the laminate was pulled while
215 the other was fixed against the concrete with a bonded region of 250 mm (EBR component) followed
216 by the transversely compressed metallic anchorage with 272 mm of length (anchorage component).

217 Firstly, the bonded region supports the increasing loads but when its maximum capacity is attained the
218 new load increments are supported by the compressed metallic anchorage. The bond strength and
219 debonding process varies between both regions as it is described in the following paragraphs.

220

221 3.1. Load-slip behaviour

222 All concrete specimens experienced a similar pattern in terms of load-slip behaviour, which is
223 represented in **Figure 4**. A first almost linear branch, governed by the EBR component, with a steep
224 slope is observed in the loaded end until EBR debonding (**Figure 4**: 0-1). During this phase, the slip
225 registered in the mid end is negligible, meaning that all the force is carried by the bonded length
226 outside the mechanical anchorage. Next, the debonding starts to occur (**Figure 4**: 1). During the
227 debonding process (**Figure 4**: 1-2), the load does not increase whilst the slip increases considerably due
228 to the elastic energy accumulated in the bonded length. At the end of the debonding phase, the mid end
229 immediately starts to register some slip; at that point, the mechanical anchorage activates. The pull-out
230 test was controlled by the displacement of the laminate loaded end and, due to the configuration of the
231 test, the transition from the EBR to the anchorage, although swift, occurred without damaging the
232 CFRP laminate and without any loss in the total pull-out force. Once all the bonded length of the
233 laminate is detached from the concrete surface, the CFRP laminate is firmly held between the clamping
234 system and the mechanical anchorage plate, facing a continuous increase in its strain and sustained
235 load. Due to the elastic behaviour of the CFRP laminate, a fairly linear load-slip response is registered

236 in all cases. Finally, in the last stages of the test (**Figure 4: 3-4**), the laminate strain continues
237 increasing but its linearity is lost due to some minor slip taking place in the mechanical anchorage and
238 the aggregate interlock that exists at the interface CFRP/concrete (debonded zone). The test typically
239 fails by CFRP rupture; consequently, LVDT-3 (free end) generally registers negligible results. The data
240 from LVDT-3 can be, however, interpreted as an indication of the level of damage inside the metallic
241 anchorage. The data registered in all three LVDTs is analysed in the following sub-chapters 3.2 and
242 3.3.

243 By subtracting the displacement obtained in LVDT 2 (mid end) from displacement obtained in LVDT
244 1 (loaded end), the effect of this minor slip derived from the mechanical anchorage can be removed
245 from the loaded end slip. As a result, a linear load-slip curve is obtained after the debonding phase (see
246 Figure 4). The average slope of each curve allows the computation of the elastic modulus of each
247 CFRP laminate and the values are similar to those obtained in the material characterization (169 GPa,
248 173 GPa and 162 GPa for the laminates of 50 mm, 80 mm and 100 mm, respectively). Also, these
249 curves showed that the influence of the aggregate interlock that exists at the deboned zone is relatively
250 small (less than 4.7%). **Finally, a line representing the axial stiffness of the CFRP laminate is also**
251 **shown in Figure 4 for comparison purposes. The load-slip curve without considering the mid end slip**
252 **compares relatively well with the axial stiffness of the CFRP.**

253 In **Figure 5**, the load-slip behaviour of all specimens is represented at the loaded end, mid end and free
254 end for comparison purposes. The dependence of laminate width is clearly observed in terms of
255 stiffness and load carrying capacity of the overall system: the wider the laminate, **the higher the**
256 **stiffness and capacity**. The influence of the level of torque can be also appreciated in the **bond shear**
257 **stress-slip curves after debonding of the EBR component**: lower values of torque provide, in general, a
258 less stiff response in terms of pullout-slip, meaning that more damage is generated inside the
259 mechanical anchorage. On the contrary, higher levels of torque cause slightly stiffer responses.
260 Therefore, specimens with the smallest level of torque (30 N·m) exhibit the highest ultimate slip and, as
261 shown in **Table 5** and **Figure 5**, as the torque level is increased, smaller values of the ultimate slip are
262 observed at the loaded-end and at the mid-end. The values of slip at the free end are only illustrative of
263 the potential movement of the laminate with respect to the metallic plate and the concrete; however, it
264 is observed that lower values of torque (i.e. 30 N·m) provide more movement at the free end of the

265 laminate, proving that the level of damage inside the metallic anchorage is higher in these cases than
266 for high torque values.

267

268 3.2. EBR component

269 3.2.1. Debonding load and fracture energy

270 The debonding load (P_{deb} , **Table 3**) is defined in this experimental programme as the load at which the
271 laminate (at the EBR component) is debonded from the concrete substrate and, consequently, the
272 mechanical anchorage starts to carry the entire load. Because the anchorage component had a length
273 higher than the effective bond length, it was possible to obtain a very stable value of the debonding
274 load (**Figure 4: 1-2**), which represents the asymptotic value of the transmissible force by an anchorage
275 of infinite length (without compressive stresses). In this experimental programme, the debonding
276 process is observed to occur sudden and abruptly in all cases. Moreover, the failure mode obtained is
277 cohesive in the concrete, a few millimetres beneath the concrete/epoxy interface, as it is well reported
278 in the literature [5].

279 In the case where the CFRP laminate and adhesive properties were identical, equal values of ultimate
280 debonding strength would be assumed for all specimens, and hence a linear dependence of P_{deb} on the
281 laminate width would be expected. According to the literature [5,12,51] the used bonded length
282 (250 mm) surpasses the theoretical effective length, L_e , in this case of 200 mm [51], needed to achieve
283 the maximum debonding load. Although different CFRP modulus of elasticity were observed, the
284 relation between the mean value of P_{deb} and the laminate width can be assumed to be linear (a constant
285 value of 0.520 kN (CoV= 8.2%) per unit length of CFRP width was obtained for all specimens).

286 In general terms, the fracture energy associated to the bond shear stress-slip law $\tau(s)$ in the bonded
287 length, G_f , can be expressed as:

$$G_f = \int_0^{\infty} \tau(s) ds \quad (3)$$

288 Assuming a stiffness in concrete much higher than the stiffness of the EBR reinforcement, the
289 equilibrium of energies can be assumed in the section where the maximum stress σ_f is applied and the
290 following relationship can be deduced for a unit length [17]:

$$\int_{A_f} \frac{1}{2} \sigma_f \varepsilon_f dA = w \int_0^{\infty} \tau(s) ds \quad (4)$$

291 Hence, a value of the fracture energy G_f corresponding to P_{deb} can be calculated as:

$$G_f = \frac{P_{deb}^2}{2E_f w A_f} \quad (5)$$

292 where A_f , E_f and w are the cross-section area, the modulus of elasticity and the width of the CFRP
 293 laminate, respectively. The values of G_f calculated according to Eq. (5), taking into account the
 294 experimental values of P_{deb} , are also shown in **Table 3**. As expected, G_f keeps almost constant for all
 295 the specimens, ranging between 0.58 and 0.71 N/mm.

296 The experimental values of G_f can be compared with the ones predicted by different analytical
 297 approaches. For this particular case, CNR [51] predictions are assumed. CNR proposes a value for the
 298 design fracture energy (Eq. (6) – in [N/mm]) depending on the concrete compressive and tensile
 299 strength (f_{cm} and f_{ctm} , respectively – in [N/mm²]), a confidence factor (FC), adopted equal to 1, a
 300 geometrical corrective factor k_b (dimensionless parameter) and an additional corrective factor taking
 301 into account the bonding system k_G (pre-cured or wet lay-up systems are considered), in [mm].”

$$G_f = \frac{k_b k_G}{FC} \sqrt{f_{cm} f_{ctm}} \quad (6)$$

302 The theoretical results obtained with Eq. (6) assuming k_G equal to 0.063 mm (mean value for a pre-
 303 cured system, [51]) are presented in **Table 3**. It is observed a reasonable good fit between theoretical
 304 and experimental values, with a slight trend to theoretically overestimate G_f . In fact, on average, G_f
 305 obtained experimentally is equal to 0.65 N/mm, whereas according to the CNR is equal to 0.69 N/mm.

306 The influence of the concrete roughness on the bond shear stress-slip behaviour has been previously
 307 reported in the literature [13], and some studies have provided a roughness coefficient to take into
 308 account its influence on G_f [10,53]. Iovinella *et al.* [10], for instance, adjusted the CNR formulation
 309 (Eq. (6)) thought a roughness factor I_R that considers the average of individual measures peak-to-valley
 310 heights and the inclination angle of the profile. A more recent study [53] has proposed an improvement
 311 on Eq. (6) to consider the effect of the roughness of the concrete surface on the calculation of the
 312 fracture energy, by only considering the average roughness, R_a (dimensionless parameter):

$$G_f = \frac{k_b k_G k_R}{FC} \sqrt{f_{cm} f_{ctm}} \quad (7)$$

$$k_R = 1.1R_a + 0.8 \quad (8)$$

313 In **Table 3**, the value of G_f taking into account the roughness coefficient is shown together with the
 314 experimental value and the one obtained by Eq. (7). It can be easily observed that for this experimental
 315 programme, the approach proposed by [53] provides a better fit to the experimental values.

316 The ultimate strength [51], defined as the maximum allowed strength before debonding assuming that
317 the provided bonded length is equal or larger to the optimal bonded length, is assumed to be:

$$f_{fdd} = \frac{1}{\gamma_{f,d}\sqrt{t_f}} \sqrt{2E_f G_f} \quad (9)$$

318 where $\gamma_{f,d}$ is a partial safety factor. **In Table 3, the ultimate strength has been calculated** considering a
319 safety factor $\gamma_{f,d}$ of 1.0 in order to obtain the theoretical value of P_{deb} and considering the theoretical
320 value of G_f obtained by Eq. (7). The η value shows the ratio between the experimental ($P_{deb,exp}$) and the
321 predicted ($P_{deb,th}$) value for P_{deb} . In general terms, the experimental value of P_{deb} is in accordance (with
322 a confidence interval of $\pm 5\%$) with the predicted by CNR taking into account the roughness coefficient
323 k_R . **Figure 6 shows the values of the debonding and the ultimate load for all the specimens, together**
324 **with theoretical predictions. The theoretical prediction of the debonding load was obtained from**
325 **equations (5) and (9). A good relation between the experimental debonding load, $P_{deb,exp}$, (grey bars)**
326 **and the predicted debonding load, $P_{deb,th}$, (black bars) can be observed.**

327

328 3.2.2. Strain profile in the CFRP laminate

329 The strain profile along the CFRP laminate in its bonded length, which in this study was assumed to be
330 250 mm, can provide information about the active transfer length at different levels of load. The strain
331 profile obtained from the L50-T30 and L80-T30 is presented in **Figure 7a** and **Figure 7b**, respectively.
332 Both graphs show that the activated length increases with the applied load, and complete debonding
333 takes place when there is no more **undeformed** bonded length. It can be seen that the strain at the
334 loaded end ($S1, x = 0$ mm) increases with the load from the beginning of the test at an almost constant
335 rate, as expected. At the beginning of the debonding process, the load is transferred to the next strain
336 gauge, and, in most cases, it is transferred to the next strain gauge in a relatively sudden pattern with
337 almost no increase in load (**Figure 7a**). In other cases, the debonding process is somehow less abrupt,
338 and the load is transmitted through the bonded length with a slight increase of its value (**Figure 7b**).
339 Once debonding has taken place, the strain in the laminate increases in a similar strain rate in all
340 positions.

341

342 3.2.1. Bond stress-slip curves

343 The local bond stress-slip curve along the bonded length can be easily derived from the strain values.
 344 The mean bond shear stress between two consecutive strain gauges ($\tau_{i+1/2}$) was calculated by
 345 equilibrium between the tensile pull-out force carried by the CFRP laminate and the shear force
 346 supported at the interface between concrete and laminate:

$$\tau_{i+1/2} = E_f t_f \frac{\varepsilon_{i+1} - \varepsilon_i}{x_{i+1} - x_i} \quad (10)$$

347 where t_f is the thickness of the CFRP laminate, ε_i and ε_{i+1} are the strain values at “ i ” and “ $i+1$ ”
 348 locations, respectively, and x_i and x_{i+1} are the locations of the strain gauges. Similarly, the slip of the
 349 CFRP laminate at the mean location “ $i+1/2$ ” ($s_{i+1/2}$) was calculated by integrating the experimental
 350 values of strain:

$$s_{i+1/2} = s_{i-1/2} + \frac{\varepsilon_i + \varepsilon_{i+1}}{2} (x_{i+1} - x_i) \quad (11)$$

351 A typical distribution of bond shear stress *versus* slip is depicted in **Figure 8**. The same figure also
 352 presents the experimental bond shear stress-slip curves, and the average experimental bond shear-slip
 353 curve. A first fairly linear ascending branch is observed in all cases up to 50% of the peak value of the
 354 bond stress τ_{\max} . The ascending branch is observed to be similar amongst the different pairs of strain
 355 gauges. After the peak bond stress is attained, the typical softening descending curve is registered,
 356 albeit the scatter of results is higher in this case. An upperbound value of 0.30 mm is considered for the
 357 maximum slip for not interfering with the results derived from the mechanical anchorage.

358 There are several approaches in the literature to model the local bond shear stress-slip law of FRP-
 359 concrete interface [54–56]. In this work, the law described in [57], adapted from [58], is adopted and
 360 calibrated to the experimental results:

$$\tau(s_p) = \frac{\bar{\tau} s_p^n}{\bar{s} (n-1) + (s_p/\bar{s})^n} \quad (12)$$

361 where τ and s_p are the interface shear stress and slip, $\bar{\tau}$ and \bar{s} represent the maximum shear stress and its
 362 corresponding slip, and $n (> 2)$ is the parameter governing the descending branch (higher values of n
 363 diminish the fracture energy of the system, whereas values lower than 2 provide negative and/or finite
 364 quantity values of the fracture energy, [57]). The resultant parameters $\bar{\tau}$, \bar{s} and n have been calibrated to
 365 the bond stress-slip law by a least-squares methodology and are summarised in **Table 4** for the tested
 366 specimens. In general terms, the resultant parameters are relatively similar to the ones obtained in [13].
 367 The maximum bond stress tends to reduce with the laminate width, being its value between 3.23 and

368 4.97 MPa. The influence of the width of FRP plate on the debonding process was recently investigated
369 in [59]. In their study, the authors conclude that the maximum stress is higher near the FRP plate edge
370 than in its centre due to the non-homogeneity of material at the mesoscale level and due to the
371 difference between the elastic modulus between FRP and concrete. Based on the width effect reported
372 by [59], variations in the maximum shear stress $\bar{\tau}$ can be expected for each laminate width because the
373 experimental values were measured in the centre of the CFRP laminate. The corresponding slip and the
374 n parameter, however, do not present a clear trend depending on the laminate width. In **Figure 9**, the
375 mean experimental bond shear stress-slip curve is depicted for each case, together with its adjusted
376 analytical expression.

377

378 **3.3. Anchorage component**

379 **3.3.1. Ultimate load and failure mode**

380 The results, in terms of ultimate load and failure mode are shown in **Table 5**. Contrary to what it was
381 obtained in [40,41], the rupture of the laminate was attained in most of the cases, proving the good
382 performance of the mechanical anchorage in the actual test setup.

383 The ultimate load P_u was defined as the load at which the whole specimen faced failure. As expected,
384 in those cases where the rupture of the CFRP laminate was attained, a clear dependence between P_u
385 and the laminate width was observed. In these cases, P_u was adequately predicted by the tensile
386 strength obtained from characterization of the CFRP laminates, and a maximum difference between the
387 predicted (from tensile tests) and experimental (from pull-out tests) P_u of 6.9% was obtained. In the
388 particular case of L80-T150 specimen, the value of ultimate load was not possible to acquire, due to
389 slippage of the laminate from the camping system, and in the case of L100-T150, the ultimate load was
390 not registered due to an acquisition problem during the last stages of the test. The only specimen that
391 faced slippage of the CFRP laminate from the mechanical anchorage system was L100-T30, at a load
392 of 280.80 kN, which was approximately 94% of the capacity of the laminate. The ultimate load is
393 presented in **Figure 6** which allow a visible comparison between the experimental results (light blue
394 bars) and the expected ultimate load (dark blue bars) considering the maximum CFRP strength.

395 The ultimate strain shown in **Table 5** is the maximum strain registered by the strain gauges all along
396 the bonded length at the ultimate load. In the cases where the rupture of the laminate is attained, its

397 value is very close to the ultimate strain obtained by the characterization of the CFRP laminate (see
398 **Table 1**), being the ratio theoretical/experimental ultimate strain between 0.92 and 1.18.

399 Based on the observed failure modes and values of normal stress attained in the CFRP laminate at the
400 ultimate load, it can be concluded that the studied anchorage system did not cause premature failure of
401 the CFRP laminate, mainly due to gripping effects.

402

403 **3.3.2. Influence of the torque level**

404 Although rupture of the CFRP laminate was the dominant failure mode, there is an intrinsic relation
405 between the compressive stress level and anchorage performance, which could be observed in the
406 present experimental programme. The ultimate slip registered at the loaded end (LVDT-1, **Figure 3**)
407 was always higher than the expected elastic deformation of the CFRP laminate in the bonded length
408 (250 mm) – between LVDT's 1 and 2 – indicated that slip at mid-end always occurred. Furthermore,
409 the ultimate slip increased with the decrease of the torque level, showing that increasing the
410 compressive stress provided by torqueing the anchorage allowed less slip inside the mechanical
411 anchorage. The same relation can be observed in the mid end (LVDT-2, **Figure 3**). For each laminate
412 width, the specimens with the smallest torque level (30 N·m, red line in **Figure 5b**) presented the
413 highest ultimate slip. In fact, the relation between the torque level and the slip in the metallic anchorage
414 can be easily observed in the mid end because, contrary to the slip registered at the loaded end, the
415 elastic deformation of the CFRP laminate can be neglected. As referred before, the slip registered in the
416 free end (LVDT-3, **Figure 5c**) shows negligible results. Contrary to L100_T30, where the failure mode
417 was slippage, the remaining specimens failed by CFRP rupture, thus making very difficult the
418 correlation between the slip registered in the free end at the maximum load and the torque level.
419 However, **Figure 5c** shows that during the pull-out test some specimens exhibit higher movement on
420 the free-end. The registered movement on LVDT-3 is related to the (increasing) degradation of the
421 bond conditions provided by the anchorage system that occur during the increase of pull-out force.
422 Here, a similar remark related to the level of torque can be attained: for the lowest torque level and,
423 consequently, the smallest compressive stress level on the anchorage component, the highest the
424 damage on the inside of the metallic anchorage is observed.

425 Finally, a measure of the level of visible damage inside the mechanical anchorage at the ultimate load
426 was analysed by separating the metallic plate from the concrete specimen at the end of the pull-out test.

427 As can be seen in **Figure 10**, there is a visible damage that can be observed over the laminate and in
428 the metallic plate. The visible damage over the laminate is composed mainly by missing fragments of
429 epoxy, which stayed glued to the metallic plate. This kind of damage wasn't observed on specimens
430 L50_T150 and L50_T200. In these two specimens, a peculiar dark stain could be observed on the
431 metallic anchor but no visible damage was observed over the laminate (in the adhesive). The dark stain
432 can be also observed in other plates, however in these two cases no fragments of epoxy were detected.
433 This area of visible damage has a rectangular shape with the same width of its respective laminate and
434 variable length. Then, the length of the visible damage was recorded and, based on the measurements,
435 the percentage of damage was accessed. The percentage of visible damage (VD) is the ratio between
436 the damaged length and the total length of the plate (**Table 5**). In general terms, the level of visible
437 damage inside the metallic plate increased with the decrease of torque, which proved the effectiveness
438 of a transversely compressed anchorage. In the case of L80-T150, the observed degree of visible
439 damage was lower than expected due to the premature failure obtained in this test. On the other hand,
440 the level of visible damage increased with the laminate width. Assuming a constant distribution of
441 compressive stress (in transverse direction) along the laminate width, it is foreseen that for the same
442 level of torque (and hence the same transverse force), a wider laminate receives less compressive stress
443 and consequently the system suffers higher degree of damage. Finally, in most of the cases, it could be
444 observed that the increase in visible damage along the laminate width was not evenly distributed, being
445 more pronounced in the centre of the CFRP (see **Figure 10**). This observation indices that there are,
446 inside the anchorage, higher axial stresses in the centre of the laminate. In fact, the prestress of the
447 anchor bolts slightly bended the anchorage plate (deformation not measured, just observed by naked
448 eye) and, consequently, produced higher compressive stress in the extremities of the laminate. This
449 bent deformation was not prevented in order to be representative of the real applications of this
450 commercial anchorage system.

451 **Figure 11** plots the influence of the compressive stress level over the average tangential stress inside
452 the anchorage for the load of failure. It should be pointed out that the area and shape of tangential stress
453 distribution inside the anchorage region could not be precisely identified. Therefore the average
454 tangential stress is based on the area of visible damage. Here, the area of visible damage is considered
455 to be the area for which the tangential stresses are developed at the joint between laminate and
456 concrete. The compressive stress level was computed based on the prestress applied in the six M16

457 anchor bolts and the area of the CFRP laminate in contact with the metallic plate. The prestress level
458 was measured with a dynamometric key and, simultaneously, in two of the six bolts of each anchorage
459 system, using strain gauges. Because the strain in the monitored anchor bolts was constantly measured
460 it was possible to observe that the **compressive stress level** was the same in the test day.

461 Because the average tangential stress and **compressive stress level** exhibit a good relation, it can be
462 foreseen that the anchorage ultimate load capacity can be increased with **the torque level applied in the**
463 **M16 anchor bolts. In Figure 11 specimens L50_T150 and L50_T200 were not represented because the**
464 **visible damage (mobilized anchorage zone) was close to zero, being the level of tangential stresses in**
465 **this zone very high.**

466 As referred before, the maximum load attained at failure corresponds to the maximum tensile capacity
467 of the FRP. In consequence, **applying a compressive stress in the anchorage region** seems to be a
468 practical solution for increasing the anchorage resistance. However, the ultimate load capacity of the
469 anchorage could be reduced due to environmental exposure, thermal or loading cycling, as is the case
470 of the observations in [40,41]. **Correia et al. [40,41] have performed durability tests on RC slabs**
471 **strengthened with prestressed CFRP laminate strips under different environmental and loading**
472 **conditions. In this work the prestressed CFRP laminates were anchored at the ends with the system**
473 **studied in the scope of the present manuscript. Different environmental conditions were considered: (i)**
474 **wet-dry cycles, (ii) moisture, (iii) freeze-thaw and (iv) thermal cycles. With the exception of the control**
475 **specimens, where the failure occurred by CFRP laminate rupture, in the remaining specimens the**
476 **failure occurred by slippage of the CFRP laminate at the end anchorages. Many reasons have been**
477 **pointed out for such results, mainly plasticization of the epoxy adhesive and thermal cycling fatigue in**
478 **the involved materials that yielded to the degradation of the bond at the interfaces. Additionally, it is**
479 **well-known that when the epoxy adhesives are submitted to temperatures higher than to the**
480 **corresponding glass transition temperature (for this type of epoxy adhesive is in the range of 55 to 60**
481 **°C), their mechanical properties are significantly decreased. This critical aspect may be decrease the**
482 **performance of mechanical anchorage system and has been observed by Firmo et al. [60]. For that**
483 **reason, further studies should be carried out.**

484

485 **4. Conclusions**

486 This paper has presented the results of an experimental programme aimed at studying the effectiveness
487 of a mechanical anchorage of EBR CFRP laminates bonded to concrete structures. For this purpose, the
488 results of 11 large-scale pullout tests comprising prismatic concrete blocks externally bonded with
489 CFRP laminates (of three different widths) and mechanically anchored (with four torque levels), have
490 been presented and discussed. From the experimental results, the following observations and
491 conclusions can be drawn:

- 492 • In general terms, the mechanical anchorage used in this experimental programme provides
493 adequate compressive stress of the CFRP laminate to the concrete substrate, regardless of the
494 torque level (30, 100, 150 or 200 N·m). However, for a laminate width of 100 mm, the lowest
495 torque level (30 N·m) yielded to slippage of the CFRP laminate;
- 496 • A typical cohesive failure in the concrete was observed in the bonded length (EBR
497 component). The debonding load increased with the laminate width. However, some
498 deviations are observed due to the different modulus of elasticity of the laminates;
- 499 • The load-slip behaviour at the loaded end showed all the typical stages during the debonding
500 process: (i) a first almost linear and steep branch, (ii) debonding of the laminate and (iii) a
501 phase where the laminate was firmly held by the mechanical anchorage plate, until rupture of
502 the laminate, or, in case of L100-T30 specimen, slippage of the laminate from the plate;
- 503 • The debonding process along the EBR bonded length was registered by the strain gauges
504 placed along the laminate, showing similar behaviour to the one reported by the literature,
505 mainly [13,17,51,53];
- 506 • A local bond shear stress-slip curve was experimentally obtained from the data registered by
507 the strain gauges for each specimen, and was adjusted to the model presented in [31],
508 obtaining an average bond shear strength, corresponding slip and the parameter governing the
509 descending branch of 4.2 MPa, 0.082 mm and 3.7;
- 510 • The majority of the tested specimens failed when the maximum capacity of the CFRP was
511 reached. By removing the anchorage plate from the specimen, an assessment of the visible
512 damage was carried out and a relation Mohr-Coulomb between the compressive stress level
513 and average shear stress at the maximum load was observed with a cohesion and friction angle
514 of 5.26 MPa and 13.7°, respectively;

515 • Over the completed test campaign, it was possible to predict an increase on the anchorage
516 capacity with the compressive stress level, expressed by the reduction of the slip at the mid
517 end.

518 Based on the obtained results it is important to, in future works, investigate the influence of transverse
519 compressive stress in the bond of externally bonded reinforcement with mechanical anchorages when
520 exterior actions are applied, namely, temperature, humidity, and load cycling since the existing
521 literature has shown a decrease of efficiency (capacity of avoiding the CFRP slippage from the
522 anchorage system) when this system is utilized in the strengthening of RC slabs.

523

524 **Acknowledgements**

525 This work was supported by FEDER funds through the Operational Program for Competitiveness
526 Factors – COMPETE and National Funds through FCT (Portuguese Foundation for Science and
527 Technology) under the project FRPLongDur POCI-01-0145-FEDER-016900 (FCT PTDC/ECM-
528 EST/1282/2014) and partly financed by the project POCI-01-0145-FEDER-007633. The first author
529 acknowledges the Spanish Government (Ministerio de Educación, Cultura y Deporte) for the grant José
530 Castillejo ref. CAS16/00288. The second author wishes also to acknowledge the grant
531 SFRH/BD/98309/2013 provided by FCT. Finally, the authors also like to thank the S&P Clever
532 Reinforcement Ibérica Lda. company for providing the materials.

533

534 **References**

- 535 [1] FIB. Externally bonded FRP reinforcement for RC structures. 2001. doi:10.1016/0262-
536 5075(85)90032-6.
- 537 [2] Teng J, Chen JF, Smith S, Lam L. FRP Strengthened RC Structures. John Wiley & Sons, Inc.;
538 2001. doi:10.1002/pi.1312.
- 539 [3] Bank LC. Composites for Construction: Structural Design with FRP Materials. John Wiley &
540 Sons, Inc.; 2006. doi:10.1002/9780470121429.
- 541 [4] Kalfat R, Smith ST. Anchorage devices used to improve the performance of reinforced
542 concrete beams retrofitted with FRP composites : state-of-the-art review. J Compos Constr
543 2013;17:14–33. doi:10.1061/(ASCE)CC.1943-5614.0000276.
- 544 [5] Chen J, Teng J. Anchorage Strength Models for FRP and Steel Plates. J Struct Eng

- 545 2001;127:784–91.
- 546 [6] Bilotta A, Ceroni F, Di Ludovico M, Nigro E, Pecce M, Manfredi G. Bond Efficiency of EBR
547 and NSM FRP Systems for Strengthening Concrete Members. *J Compos Constr* 2011;15:757–
548 72. doi:10.1061/(ASCE)CC.1943-5614.0000204.
- 549 [7] Ceroni F, Pecce M. Evaluation of Bond Strength in Concrete Elements Externally Reinforced
550 with CFRP Sheets and Anchoring Devices. *J Compos Constr* 2010.
551 doi:10.1061/(ASCE)CC.1943-5614.0000118.
- 552 [8] El-Hacha R, Wight R, Green MF. Prestressed fibre-reinforced polymer laminates for
553 strengthening structures. *Prog Struct Eng Mater* 2001;3:111–21. doi:10.1002/pse.76.
- 554 [9] Oehlers DJ, Visintin P, Lucas W. Fundamental mechanics governing FRP-retrofitted RC
555 beams with anchored and prestressed FRP plates. *J Compos Constr* 2016;20:4015072.
556 doi:10.1061/(ASCE)CC.
- 557 [10] Iovinella I, Prota A, Mazzotti C. Influence of surface roughness on the bond of FRP laminates
558 to concrete. *Constr Build Mater* 2013. doi:10.1016/j.conbuildmat.2012.09.112.
- 559 [11] Mazzotti C, Bilotta A, Carloni C, Ceroni F, D’Antino T, Nigro E, et al. Bond between EBR
560 FRP and concrete. In: Pellegrino C, Sena-Cruz J, editors. *Des. Proced. Use Compos. Strength.*
561 *Reinf. Concr. Struct. State-of-the-Art Rep. RILEM Tech. Comm. 234-DUC*, Dordrecht:
562 Springer Netherlands; 2016, p. 39–96. doi:10.1007/978-94-017-7336-2_3.
- 563 [12] Seracino R, Raizal Saifulnaz MR, Oehlers DJ. Generic Debonding Resistance of EB and NSM
564 Plate-to-Concrete Joints. *J Compos Constr* 2007;11:62–70. doi:10.1061/(ASCE)1090-
565 0268(2007)11:1(62).
- 566 [13] Mazzotti C, Savoia M, Ferracuti B. A new single-shear set-up for stable debonding of FRP-
567 concrete joints. *Constr Build Mater* 2009;23:1529–37. doi:10.1016/j.conbuildmat.2008.04.003.
- 568 [14] Sena-Cruz JM, Barros JAO. Bond between Near-surface mounted carbond-fiber reinforced
569 polymer laminate strips and concrete. *J Compos Constr* 2004;8:519–27.
- 570 [15] De Lorenzis L, Teng JG. Near-surface mounted FRP reinforcement: An emerging technique
571 for strengthening structures. *Compos Part B Eng* 2007;38:119–43.
572 doi:10.1016/j.compositesb.2006.08.003.
- 573 [16] Coelho MRF, Sena-Cruz JM, Neves LAC. A review on the bond behavior of FRP NSM
574 systems in concrete. *Constr Build Mater* 2015;93:1157–69.

- 575 doi:10.1016/j.conbuildmat.2015.05.010.
- 576 [17] Ceroni F, Pecce M, Bilotta A, Nigro E. Bond behavior of FRP NSM systems in concrete
577 elements. *Compos Part B Eng* 2012;43:99–109. doi:10.1016/j.compositesb.2011.10.017.
- 578 [18] Michels J, Barros J, Costa I, Sena-Cruz J, Czaderski C, Giacomini G, et al. Prestressed FRP
579 Systems. In: Pellegrino C, Sena-Cruz J, editors. *Des. Proced. Use Compos. Strength. Reinf.*
580 *Concr. Struct. State-of-the-Art Rep. RILEM Tech. Comm. 234-DUC*, Dordrecht: Springer
581 Netherlands; 2016, p. 263–301. doi:10.1007/978-94-017-7336-2_7.
- 582 [19] Michels J, Sena-Cruz J, Czaderski C, Motavalli M. Structural Strengthening with Prestressed
583 CFRP Strips with Gradient Anchorage. *J Compos Constr* 2013;17:651–61.
584 doi:10.1061/(ASCE)CC.1943-5614.0000372.
- 585 [20] Smith ST, Teng JG. Shear-Bending Interaction in Debonding Failures of FRP-Plated RC
586 Beams. *Adv Struct Eng* 2003;6:183–99. doi:10.1260/136943303322419214.
- 587 [21] Al-Amery R, Al-Mahaidi R. Coupled flexural–shear retrofitting of RC beams using CFRP
588 straps. *Compos Struct* 2006;75:457–64. doi:10.1016/J.COMPSTRUCT.2006.04.037.
- 589 [22] Pham HB, Al-Mahaidi R. Prediction Models for Debonding Failure Loads of Carbon Fiber
590 Reinforced Polymer Retrofitted Reinforced Concrete Beams. *J Compos Constr* 2006.
591 doi:10.1061/(ASCE)1090-0268(2006)10:1(48).
- 592 [23] Yalim B, Kalayci AS, Mirmiran A. Performance of FRP-Strengthened RC Beams with
593 Different Concrete Surface Profiles. *J Compos Constr* 2008. doi:10.1061/(ASCE)1090-
594 0268(2008)12:6(626).
- 595 [24] Garden HN, Hollaway LC. An experimental study of the influence of plate end anchorage of
596 carbon fibre composite plates used to strengthen reinforced concrete beams. *Compos Struct*
597 1998;42:175–88. doi:10.1016/S0263-8223(98)00070-1.
- 598 [25] Spadea G, Bencardino F, Swamy RN. Structural Behavior of Composite RC Beams with
599 Externally Bonded CFRP. *J Compos Constr* 1998. doi:10.1061/(ASCE)1090-
600 0268(1998)2:3(132).
- 601 [26] Jensen AP, Petersen CG, Poulsen E, Ottosen C, Thorsen T. On the anchorage to concrete of
602 sika carbodur CFRP strips. *Congr. Creat. with Concr.*, London.: Thomas Telford London.;
603 1999.
- 604 [27] Duthinh D, Starnes M. Strengthening of reinforced concrete beams with carbon FRP. *Compos*

- 605 Constr 2001;1:493–498.
- 606 [28] Wu Y-F, Huang Y. Hybrid Bonding of FRP to Reinforced Concrete Structures. *J Compos*
607 *Constr* 2008. doi:10.1061/(ASCE)1090-0268(2008)12:3(266).
- 608 [29] Lam L, Teng JG. Strength of RC Cantilever Slabs Bonded with GFRP Strips. *J Compos Constr*
609 2001. doi:10.1061/(ASCE)1090-0268(2001)5:4(221).
- 610 [30] Eshwar N, Ibell TJ, Nanni A. Effectiveness of CFRP Strengthening on Curved Soffit RC
611 Beams. *Adv Struct Eng* 2005;8:55–68. doi:10.1260/1369433053749607.
- 612 [31] Micelli F, Rizzo A, Galati D. Anchorage of composite laminates in RC flexural beams. *Struct*
613 *Concr* 2010;11:117–26. doi:10.1680/stco.2010.11.3.117.
- 614 [32] Zhang HW, Smith ST. Influence of FRP anchor fan configuration and dowel angle on
615 anchoring FRP plates. *Compos Part B Eng* 2012;43:3516–27.
616 doi:10.1016/J.COMPOSITESB.2011.11.072.
- 617 [33] Zhang HW, Smith ST. FRP-to-concrete joint assemblages anchored with multiple FRP
618 anchors. *Compos Struct* 2012;94:403–14. doi:10.1016/J.COMPSTRUCT.2011.07.025.
- 619 [34] Zhang HW, Smith ST, Kim SJ. Optimisation of carbon and glass FRP anchor design. *Constr*
620 *Build Mater* 2012;32:1–12. doi:10.1016/J.CONBUILDMAT.2010.11.100.
- 621 [35] Smith ST. Strengthening of concrete, metallic and timber construction materials with FRP
622 composites. *Adv. FRP Compos. Civ. Eng. Proc., 5th Int. Conf. FRP Compos. Civ. Eng. CICE*
623 2010, Beijing: Tsinghua University Press; 2010.
- 624 [36] Michels J, Sena-Cruz J, Christen R, Czaderski C, Motavalli M. Mechanical performance of
625 cold-curing epoxy adhesives after different mixing and curing procedures. *Compos Part B Eng*
626 2016;98:434–43. doi:10.1016/j.compositesb.2016.05.054.
- 627 [37] Meier U, Stöcklin I. A novel carbon fibre reinforced polymer (CFRP) system for post-
628 strengthening. *Int. Conf. Concr. Repair Rehabil. Retrofit., Cape Town, South Africa: 2005.*
- 629 [38] Aslam M, Shafiq P, Jumaat MZ, Shah SNR. Strengthening of RC beams using prestressed
630 fiber reinforced polymers – A review. *Constr Build Mater* 2015;82:235–56.
631 doi:10.1016/J.CONBUILDMAT.2015.02.051.
- 632 [39] You YC, Choi KS, Kim J. An experimental investigation on flexural behavior of RC beams
633 strengthened with prestressed CFRP strips using a durable anchorage system. *Compos Part B*
634 *Eng* 2012;43:3026–36. doi:10.1016/j.compositesb.2012.05.030.

- 635 [40] Correia L, Teixeira T, Michels J, Almeida JAPP, Sena-Cruz J. Flexural behaviour of RC slabs
636 strengthened with prestressed CFRP strips using different anchorage systems. *Compos Part B*
637 *Eng* 2015;81:158–70. doi:10.1016/j.compositesb.2015.07.011.
- 638 [41] Correia L, Sena-Cruz J, Michels J, França PM, Pereira E, Escusa G. Durability of RC slabs
639 strengthened with prestressed CFRP laminate strips under different environmental and loading
640 conditions. *Compos Part B Eng* 2017;125:71–88.
641 doi:https://doi.org/10.1016/j.compositesb.2017.05.047.
- 642 [42] Yang D-S, Park S-K, Neale KW. Flexural behaviour of reinforced concrete beams strengthened
643 with prestressed carbon composites. *Compos Struct* 2009;88:497–508.
644 doi:10.1016/J.COMPSTRUCT.2008.05.016.
- 645 [43] Hansen CS, Schmidt JW, Stang H. Transversely compressed bonded joints. *Compos Part B*
646 *Eng* 2012;43:691–701. doi:https://doi.org/10.1016/j.compositesb.2011.11.049.
- 647 [44] CEB-FIP. Model Code for Concrete Structures 2010. 2013.
- 648 [45] Biscaia HC, Chastre C, Silva MAG. Bond-slip model for FRP-to-concrete bonded joints under
649 external compression. *Compos Part B Eng* 2015;80:246–59.
650 doi:https://doi.org/10.1016/j.compositesb.2015.06.004.
- 651 [46] Eurocode. BS EN 1992-2:2005 - Eurocode 2: Design of concrete structures - Part 2: Concrete
652 bridges - Design and detailing rules. Eurocode 2 2005.
- 653 [47] NP EN 12390-3. Testing hardened concrete. Part 3: Compressive strength of test specimens.
654 Caparica; IPQ-Instituto Português de Qualidade: 2011.
- 655 [48] LNEC E397. Concrete - Determination of elasticity Young modulus under compression. 1993.
- 656 [49] ISO 527-5. Plastics - Determination of tensile properties - Part 5: Test conditions for
657 unidirectional fibre-reinforced plastic composites. Genève; ISO - International Organization for
658 Standardization: 1997.
- 659 [50] Silva P, Fernandes P, Sena-Cruz J, Xavier J, Castro F, Soares D, et al. Effects of different
660 environmental conditions on the mechanical characteristics of a structural epoxy. *Compos Part*
661 *B Eng* 2016;88:55–63. doi:10.1016/j.compositesb.2015.10.036.
- 662 [51] CNR. Guide for the design and construction of externally bonded FRP systems for
663 strengthening existing structures. 2013.
- 664 [52] Myers J, Shen X, Maerz N. Effect of varied surface roughness, putty thickness and concrete

665 strength on the interfacial bond strength of FRP to concrete. Transp. Res. board, 2007.

666 [53] Soares S, Cruz JR, Fernandes P, Sena-Cruz J. Bond behavior of EBR CFRP systems in
667 concrete : influence of surface preparation. Proc. 6th Asia-Pacific Conf. FRP Struct.,
668 Singapore: 2017.

669 [54] Lu XZ, Teng JG, Ye LP, Jiang JJ. Bond-slip models for FRP sheets/plates bonded to concrete.
670 Eng Struct 2005;27:920–37. doi:10.1016/j.engstruct.2005.01.014.

671 [55] Neubauer U, Rostasy FS. Bond Failure of Concrete Fiber Reinforced Polymer Plates at
672 Inclined Cracks—Experiments and Fracture Mechanics Model. ACI Spec Publ 1999;188:369–
673 82.

674 [56] Monti G, Renzelli M, Luciani P. FRP ADHESION IN UNCRACKED AND CRACKED
675 CONCRETE ZONES. Sixth Int. Symp. FRP Reinf. Concr. Struct. - FRPRSC-6., 2003, p. 183–
676 92. doi:10.1142/9789812704863_0015.

677 [57] Ferracuti B, Savoia M, Mazzotti C. Interface law for FRP-concrete delamination. Compos
678 Struct 2007;80:523–31. doi:10.1016/j.compstruct.2006.07.001.

679 [58] Popovics S. A numerical approach to the complete stress strain curve for concrete. Cem Concr
680 Res 1973;3:583–99.

681 [59] Xu T, He ZJ, Tang CA, Zhu WC, Ranjith PG. Finite element analysis of width effect in
682 interface debonding of FRP plate bonded to concrete. Finite Elem Anal Des 2015;93:30–41.
683 doi:10.1016/j.finel.2014.08.009.

684 [60] Firmo JP, Correia JR, Pitta D, Tiago C, Arruda MRT. Experimental characterization of the
685 bond between externally bonded reinforcement (EBR) CFRP strips and concrete at elevated
686 temperatures. Cem Concr Compos 2015;60:44–54.
687 doi:<https://doi.org/10.1016/j.cemconcomp.2015.02.008>.

688

689

Figure captions

690

691

692 **Figure 1.** Strengthening procedure.

693 **Figure 2.** 2D drawing of the anchorage plate (unit in [mm]).

694 **Figure 3.** Test set-up: (a) photo of the set-up, (b) side view and (c) top view of the test set-up and
695 instrumentation (units in [mm]).

696 **Figure 4.** Typical load-slip at the loaded end and mid end.

697 **Figure 5.** Load-slip curves (a) at the loaded end, (b) at mid end, and (c) at free end.

698 **Figure 6.** Debonding and ultimate load.

699 **Figure 7.** Strain profile in the CFRP laminate for (a) L50-T30, (b) L80-T30. Note: exceptionally, in
700 L50-T30 six strain gauges spaced by 50 mm were used.

701 **Figure 8.** Typical adjustment curve of local bond shear stress–slip law.

702 **Figure 9.** Experimental mean and adjusted local bond shear stress–slip law for (a) L50, (b) L80 and (c)
703 L100 specimens.

704 **Figure 10.** Damage level observed in each anchorage plate.

705 **Figure 11.** Effect of transverse confinement in the average tangential stress.

706

707

Table captions

708

709 **Table 1.** Mechanical properties of the CFRP laminates (mean values).

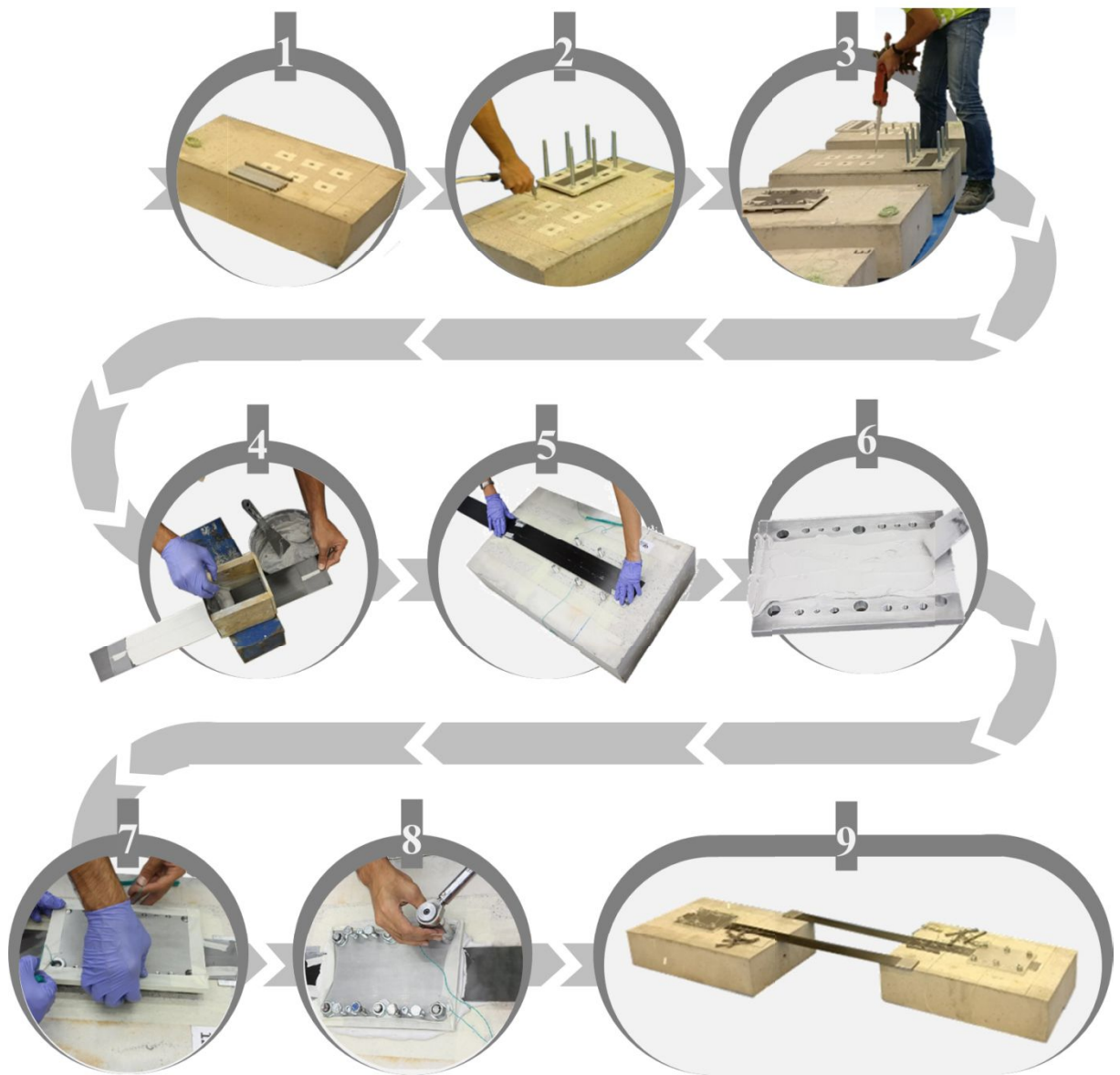
710 **Table 2.** Concrete surface roughness.

711 **Table 3.** Experimental debonding loads and comparison with analytical predictions.

712 **Table 4.** Experimental parameters for adjustment of the bond stress-slip law in Eq. (10).

713 **Table 5.** Experimental values at ultimate and mode of failure.

714



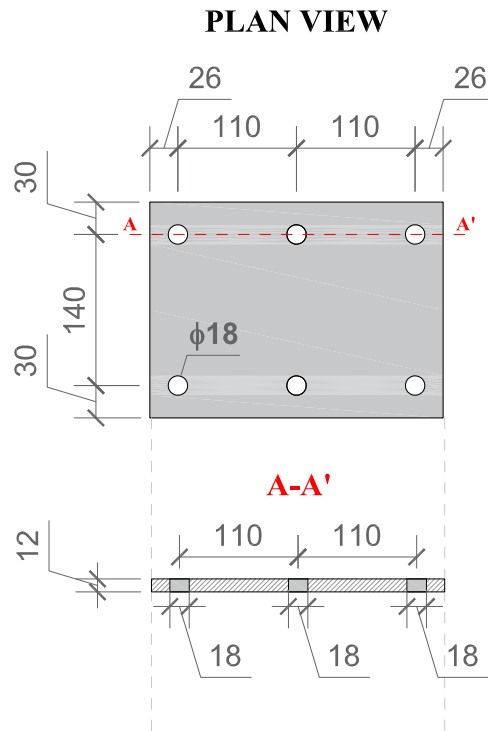
715

716

717

718

Figure 1. Strengthening procedure.



720

721

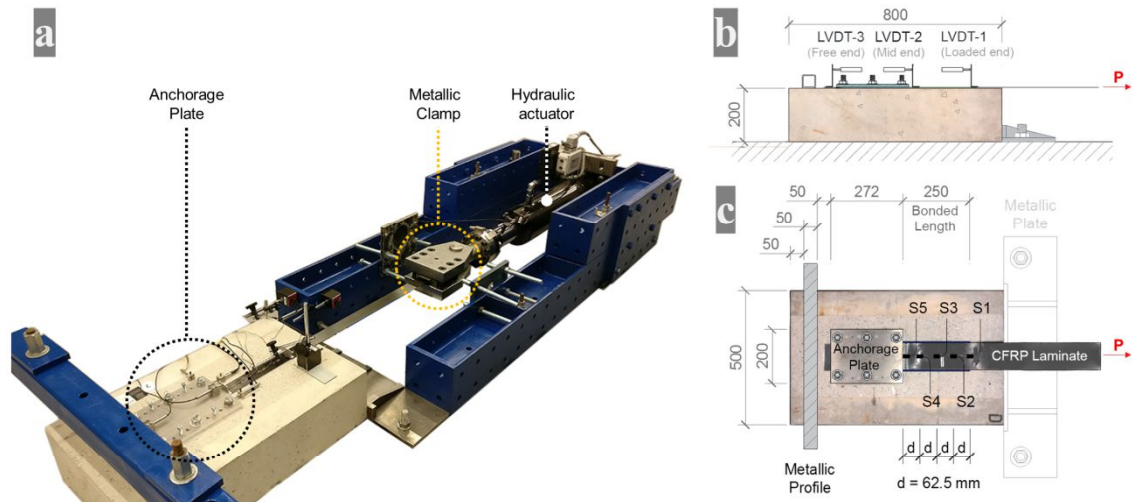
722

723

724

Figure 2. 2D drawing of the anchorage plate (units in [mm]).

725



726

727

728

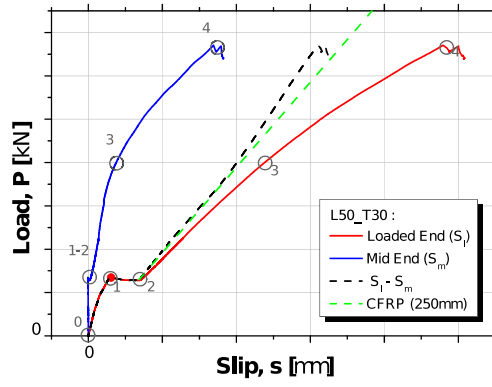
Figure 3. Test set-up: (a) photo of the set-up, (b) side view and (c) top view of the test set-up and

729

instrumentation (units in [mm]).

730

731

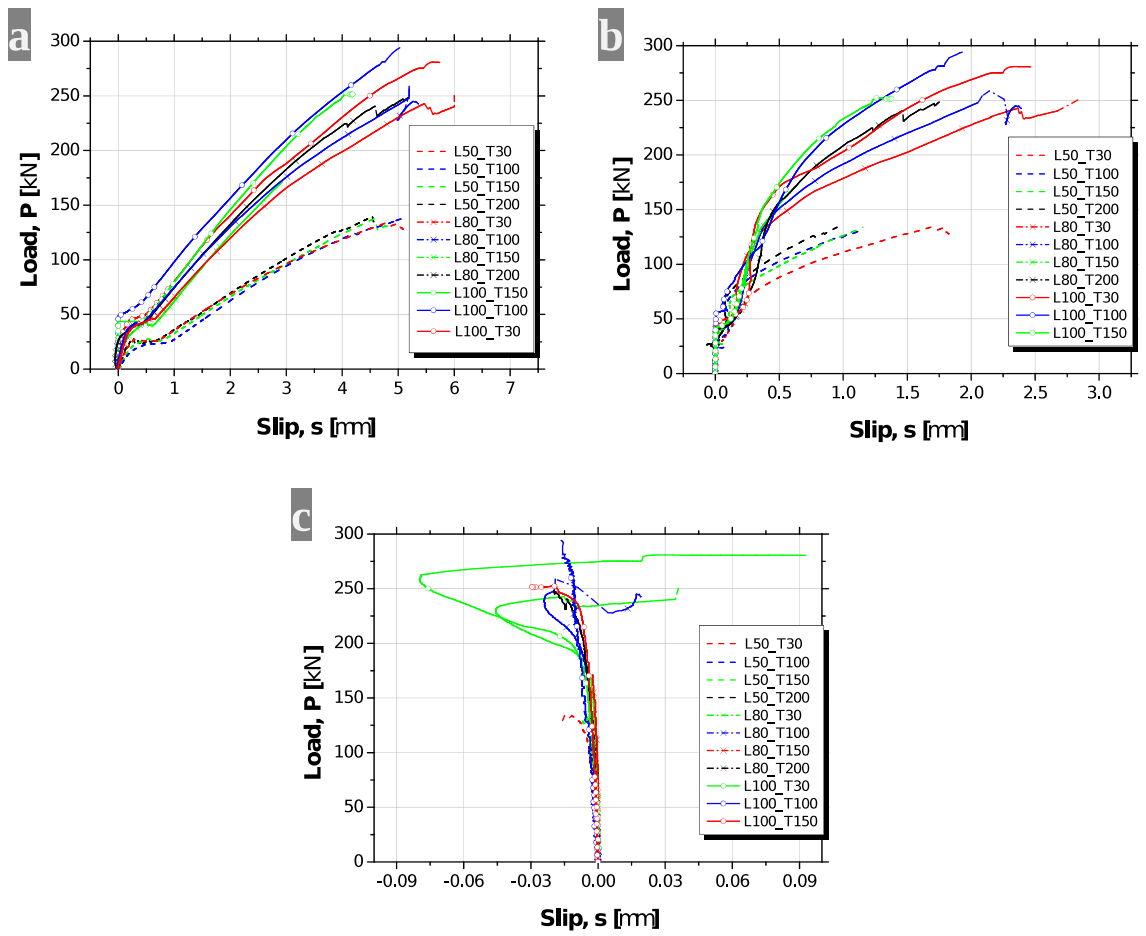


732

733

Figure 4. Typical load-slip at the loaded end and mid end (L50_T30).

734

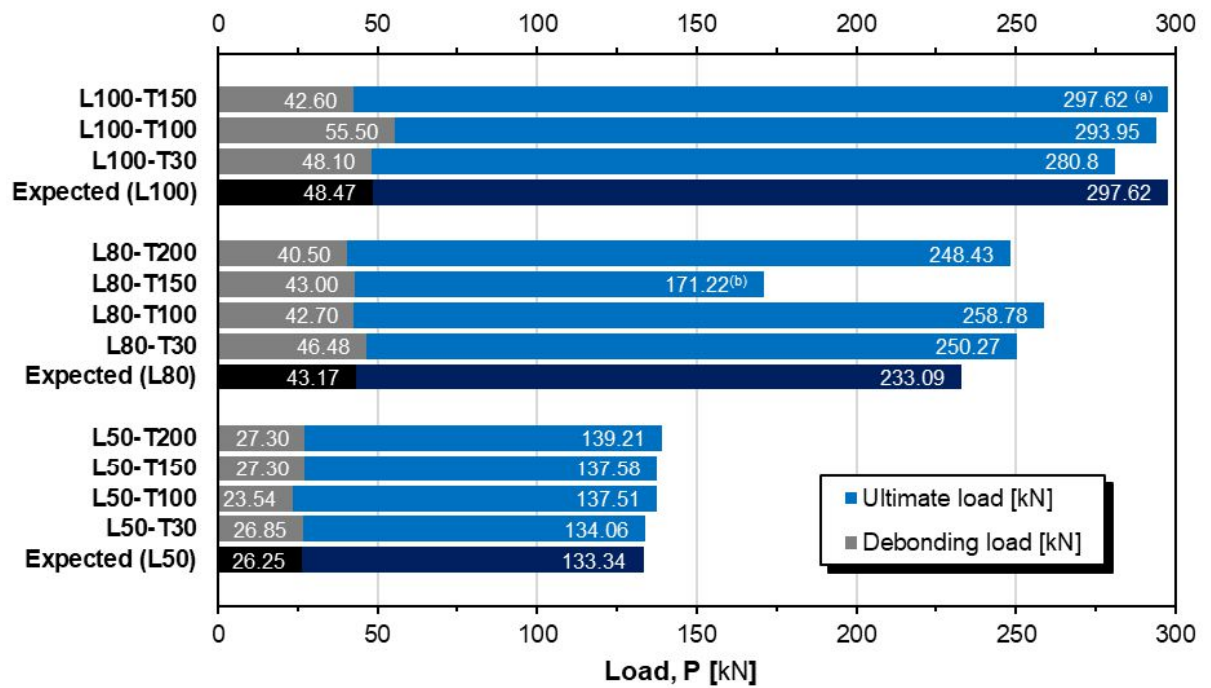


736

737

Figure 5. Load-slip curves (a) at loaded end, (b) at mid end, and (c) at free end.

738



Note: ^(a)The the ultimate load was not registered due to technical problema (data aquisition system). This value is the expected value, considering the observed failure mode (CFRP rupture). ^(b)Premature CFRP slippage from the clamping system.

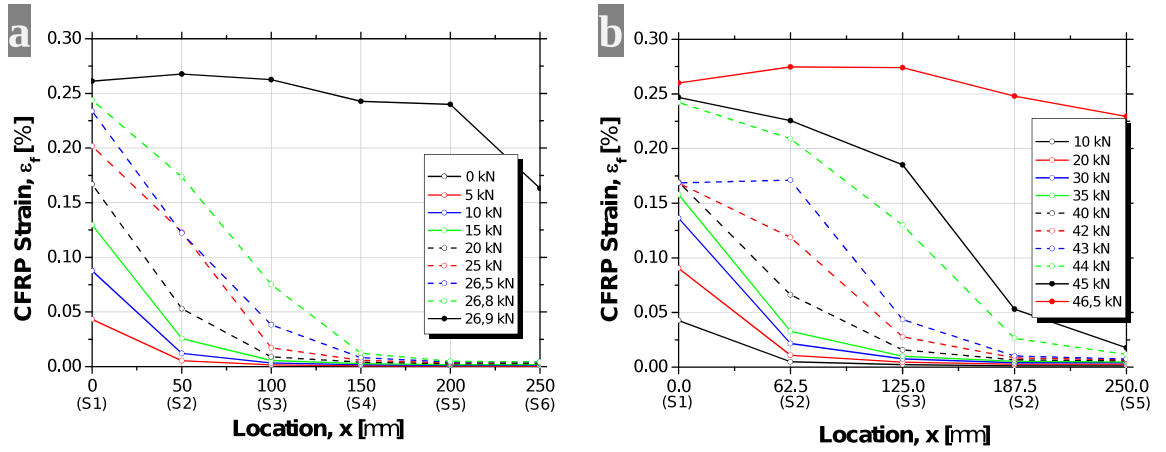
740

741

Figure 6. Debonding load and ultimate load.

742

743



744

745

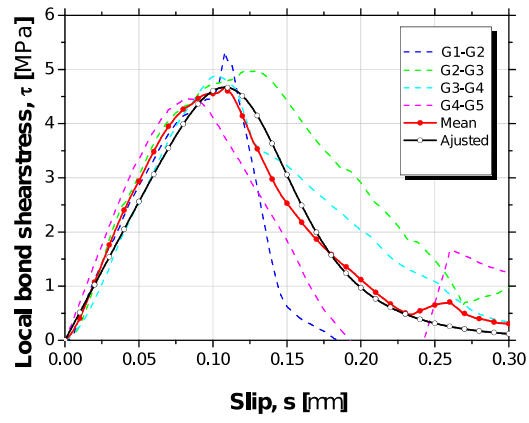
Figure 7. Strain profile in the CFRP laminate for (a) L50-T30, (b) L80-T30. Note:

746

exceptionally, in L50-T30 six strain gauges spaced by 50 mm were used.

747

748



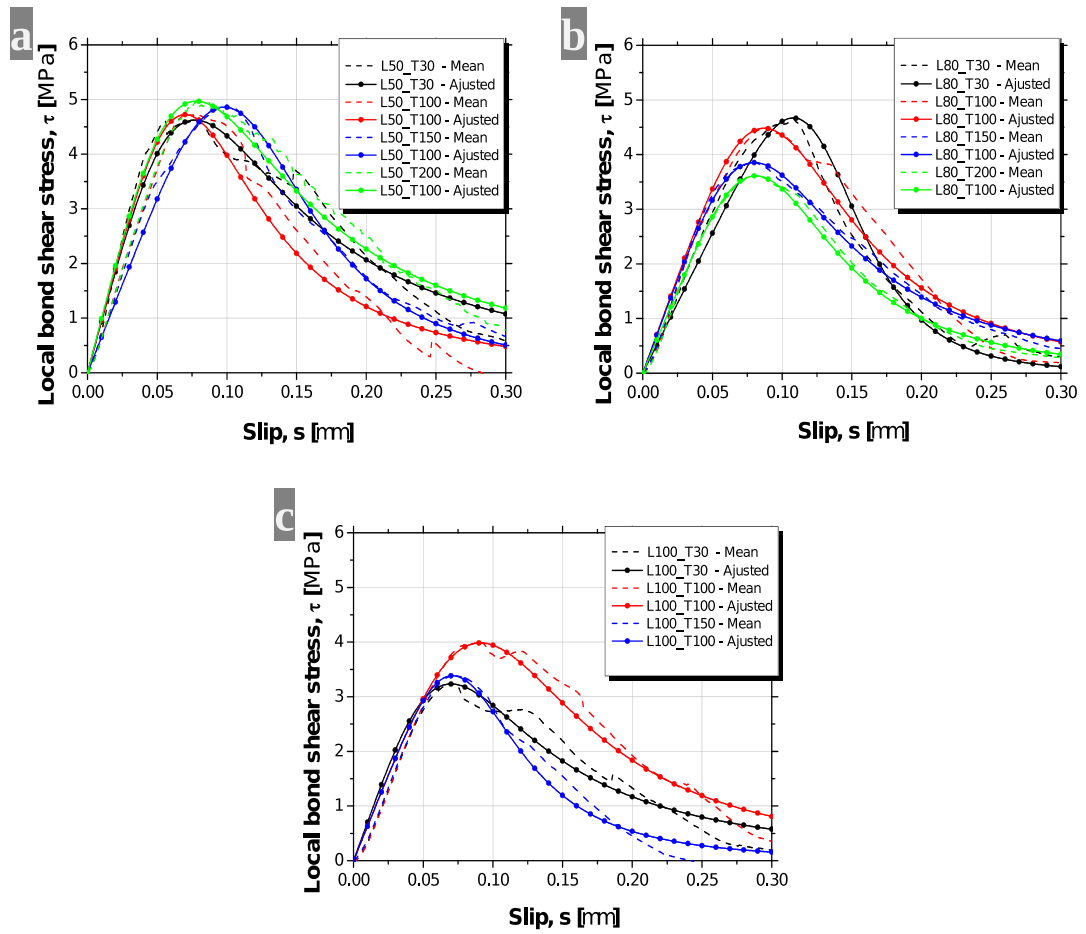
749

750

Figure 8. Typical adjustment curve of local bond shear stress – slip law (L80-T30).

751

752



753

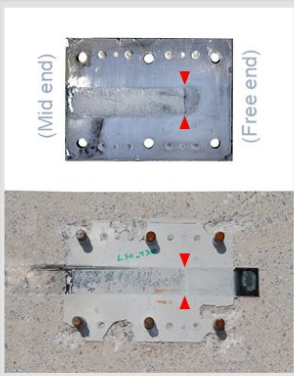
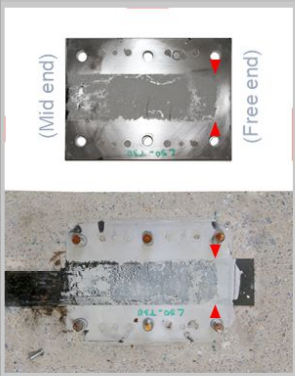
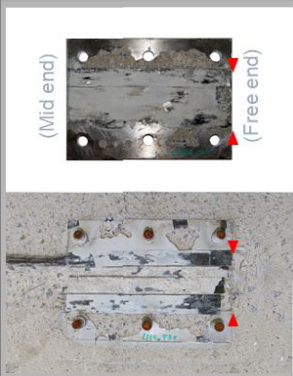
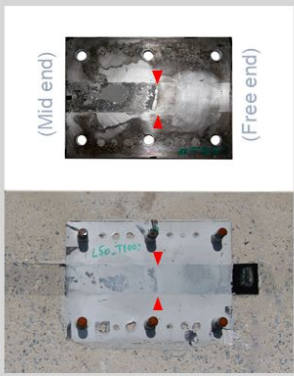
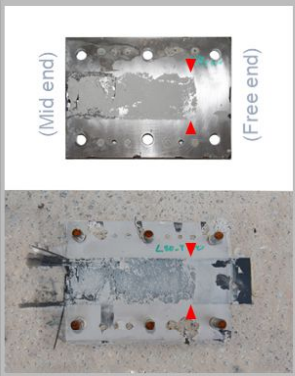
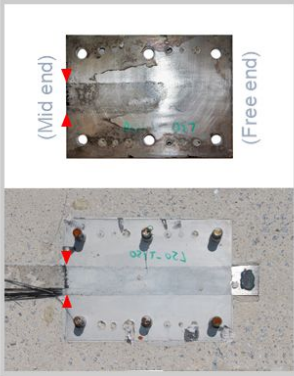
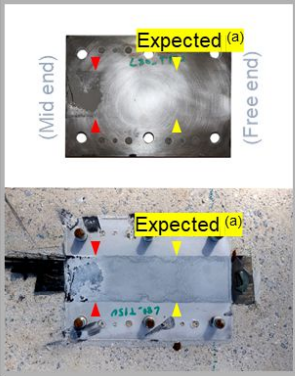
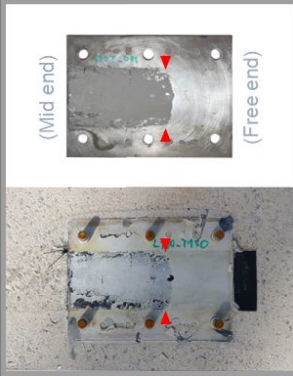
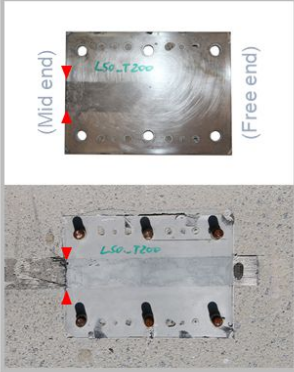
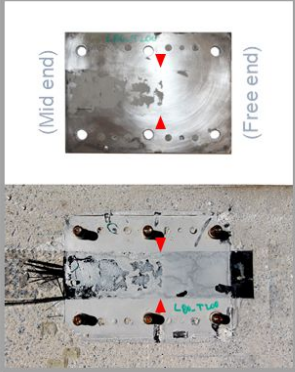
754 **Figure 9.** Experimental mean and adjusted local bond shear stress–slip law for (a) L50, (b) L80 and (c)

755

L100 specimens.

756

757

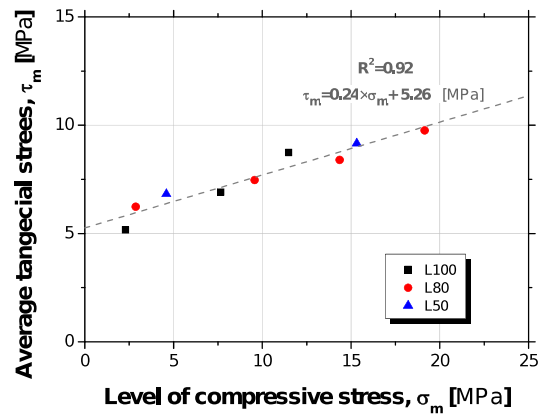
	Laminate Geometry: 50 mm × 1.2 mm (L50)	Laminate Geometry: 80 mm × 1.2 mm (L80)	Laminate Geometry: 100 mm × 1.2 mm (L100)
Torque level: 30 N·m			
Torque level: 100 N·m			
Torque level: 150 N·m			
Torque level: 200 N·m			

Note: ^(a) Estimation based on the observation of the damage zones of specimens L80_T100 and L80_T200

758

759

Figure 10. Damage level observed in each anchorage plate.



760

761

762

763

Figure 11. Effect of transverse compressive stress in the tangential stress.

764 **Table 1.** Mechanical properties of the CFRP laminates (mean values).

Laminate	Laminate width [mm]	Modulus of elasticity [GPa]	Tensile strength [MPa]	Ultimate strain [mm/m]
L50	50	176.4 (2.0%)	2222.4 (4.7%)	12.5 (2.2%)
L80	80	170.5 (0.3%)	2428.0 (4.6%)	14.6 (6.7%)
L100	100	169.4 (1.4%)	2480.2 (4.0%)	14.6 (5.8%)
Note: the values between parentheses are the corresponding CoV.				

765

766 **Table 2.** Concrete surface roughness.

	R_a [mm]	R_q [mm]	R_v [mm]	R_p [mm]	R_t [mm]
Minimum	0.116	0.147	-1.573	0.534	1.098
Maximum	0.244	0.296	-0.374	2.678	3.525
Average	0.167	0.217	-0.888	0.955	1.843
CoV	19.03%	17.94%	-26.24%	41.17%	25.35%
Note: R_a - arithmetic average of absolute values; R_q - root mean squared; R_v - maximum valley depth; R_p - maximum peak height; R_t - maximum height of the profile.					

767

768

Table 3. Experimental debonding loads and comparison with analytical predictions.

Specimen	$P_{deb,exp}$ [kN]	$P_{deb,exp}$ [kN]	$G_{f,exp}$ [N/mm] (Eq. 5)	$G_{f,th}$ [N/mm] (CNR, Eq. 6)	$G_{f,th}$ [N/mm] (Eq. 7)	$P_{deb,th}$ [kN] (Eq. 9)	η
L50-T30	26.85	26.25 (6.0%)	0.65	0.69	0.64	26.02	1.01
L50-T100	23.54						
L50-T150	27.30						
L50-T200	27.30						
L80-T30	46.48	43.17 (5.0%)	0.71	0.69	0.64	40.94	1.05
L80-T100	42.70						
L80-T150	43.00						
L80-T200	40.50						
L100-T30	48.10	48.73 (10.8%)	0.58	0.69	0.64	51.00	0.96
L100-T100	55.50						
L100-T150	42.60						
Note: the values between parentheses are the corresponding CoV.							

Table 4. Experimental parameters for adjustment of the bond stress-slip law in Eq. (12).

Specimen	$\bar{\tau}$ [MPa]	\bar{s} [mm]	n	$\bar{\tau}$ [MPa]	\bar{s} [mm]	n
L50-T30	4.62	0.077	2.8	4.79 (2.74%)	0.081 (12.91%)	3.33 (18.46%)
L50-T100	4.72	0.070	3.4			
L50-T150	4.86	0.098	4.3			
L50-T200	4.97	0.078	2.8			
L80-T30	4.67	0.108	6.4	4.15 (10.49%)	0.089 (12.69%)	4.30 (28.53%)
L80-T100	4.48	0.087	3.7			
L80-T150	3.85	0.080	3.3			
L80-T200	3.61	0.081	3.8			
L100-T30	3.23	0.070	2.9	3.53 (9.18%)	0.077 (12.51%)	3.43 (14.53%)
L100-T100	3.98	0.091	3.3			
L100-T150	3.38	0.071	4.1			
Note: the values between parentheses are the corresponding CoV.						

Table 5. Experimental values at ultimate and mode of failure.

Specimen	P_u [kN]	$P_{u,ave}$ [kN]	ϵ_u [10^{-3}]	$\epsilon_{u,ave}$ [10^{-3}]	$s_{u,l}$ [mm]	VD [%]	Failure mode
L50-T30	134.06	137.09	12.95	13.33	5.09	72.22	R-CFRP
L50-T100	137.51		13.39		5.06	55.19	R-CFRP
L50-T150	137.58		13.53		4.91	0.00	R-CFRP
L50-T200	139.21		13.44		4.57	0.00	R-CFRP
L80-T30	250.27	252.49 ^(d)	14.06	14.68 ^(d)	6.00	92.22	R-CFRP
L80-T100	258.78		15.10		5.36	79.63	R-CFRP
L80-T150	171.22		9.66		2.93	22.96 ^(a)	-- ^(a)
L80-T200	248.43		14.89		5.18	58.51	R-CFRP
L100-T30	280.80	295.79 ^(c)	13.36	13.75 ^(c)	5.74	100.00	Slippage ^(b)
L100-T100	293.95		15.13		5.03	-	R-CFRP
L100-T150	297.62 ^(c)		12.37		4.19	62.59	R-CFRP

Note: P_u – Ultimate load; $P_{u,ave}$ – Average ultimate load; ϵ_u – Ultimate strain; $\epsilon_{u,ave}$ – Average ultimate strain $s_{u,l}$ – Ultimate slip at the loaded end; VD – Percentage of visible damage; ^aPremature slippage from the clamping system; ^bSlippage from the anchorage system; ^cThe ultimate load was not registered due to a technical problem. This value corresponds to the theoretically expected result; ^dThe specimens L80-T150 and L100-T30 were not included in the assessment of the corresponding parameters.